SBA-15 modified by incorporation of alkali metals. Effect of its structural changes on the catalytic properties of Fe/SBA-15 system in the Fischer-Tropsch synthesis.

Leonardo A. Cano[a], María V. Cagnoli[b], José F. Bengoa*[b], and Sergio G. Marchetti[b]

[a] Dr. L.A. Cano
División Materiales Compuestos Termoplásticos
INTEMA, CONICET
Av. Colón 10850, Mar del Plata, 7600, Argentina

[b] Dr. M.V. Cagnoli, Dr J.F. Bengoa, Prof. Dr. S.G. Marchetti
CINDECA, CONICET, CICPBA, UNLP.
Calle 47 Nº 257, La Plata 1900, Argentina.
Email: bengoajf@quimica.unlp.edu.ar

Supporting information for this article is given via a link at the end of the document.

Abstract: A mesoporous SBA-15 solid was doped with Li, K or Cs. These systems were used as supports of iron nanoparticles and each composite was utilized as catalyst in the Fischer-Tropsch synthesis. After the activation treatment the same Fe species were detected in all solids: Fe_3O_4, α-Fe and Fe^{2+} inside SBA-15 walls. However, the species percentages and their distribution were different according to the dopant present. In all "working" catalysts a mixture of carbides ε -$Fe_{2.2}C$ and χ-Fe_2C_5, Fe_3O_4 and ions Fe^{+2} inside the SBA-15 walls were found. Alkali cations produce different amount and strength of basic sites. At 1 atm and T=703 K, the catalytic activity order was: Li> K> no doped > Cs and the alkali metals favored the production of olefins. At 20 atm, the activity was considerably higher, even at a temperature as low as 543 K, which was attributed to structural properties of the support and to diffusional effects. All catalysts showed a promising hydrocarbon production in the gasoline range. The influence of alkali metals was discussed in terms of electrostatic effects and the limited hydrocarbon chain growth was attributed to the control over size of active iron species.

Introduction

The depletion of crude oil has stimulated the utilization of nonpetroleum feedstocks including coal, natural gas, shale gas, coal-bed methane biogas, and biomass to produce liquid fuels and chemicals. One of the most practical ways for the transformation of nonpetroleum carbon resources is the production of synthesis gas (syngas, $CO+H_2$) by gasification in a first step, and then, the conversion of syngas into liquid fuels using the Fischer-Tropsch Synthesis (FTS). This process is a stepwise polymerization reaction and the products follow, in general, the Anderson-Schulz-Flory distribution. Although the FTS has been extensively studied for more than fifty years, recently, the research in this field has been increased, showing a renewed interest [1].

The problems associated with current oil extraction and processing technologies, the more stringent environmental regulations and the need for new investments in the refinery sector, makes the process of converting syngas to liquid hydrocarbons more interesting and viable for the industrial production. Therefore, efforts to increase basic and applied knowledge in FTS appear to be attractive. Different metals are active in this synthesis; however, due to its costs and availability, catalysts based on Fe and Co are the usually commercial used for this process [2]. When iron is employed, the FTS occurs simultaneously with the water–gas shift (WGS) reaction. It consumes CO and water (by-product of FTS) and produces additional H_2 and CO_2. For this reason, iron catalysts are the best choice when a syngas poor in hydrogen is used. This situation occurs if the syngas is produced by gasification of coal or biomass. Besides, iron catalysts are preferred to cobalt ones, since they have lower cost, selectivity to methane and sensitivity to poisons, and higher flexibility to lead the selectivity to alkenes, oxygenates, or branched hydrocarbons, depending on the promoters or the operative variables used [3]. A large literature about Fe catalysts is available; however, the chemical states of the active sites and the relevant nano effects, in supported systems, are not fully understood. A deep knowledge of these behaviors could help to the understanding of the reaction mechanism and consequently to the development of a new generation of catalysts [4].

Alkali metals, like potassium, are commonly added, as chemical promoters, to different iron catalysts: precipitated, fused and supported. It has been reported that alkali metals increase FTS and WGS activities, and selectivity to olefins and long chain hydrocarbons [5, 6]. Ngantsoue-Hoc et al. [7] studied the impact of different alkali promoters on FTS performances using precipitated Fe-Si catalysts. They found that K was the best promoter, increasing the CO conversion rate at all conversion levels in comparison with the unpromoted catalyst. Instead, Li and Na improved CO conversion at low to moderate conversion values; however, at high conversion levels, they were not effective or even inhibited the CO conversion. These discrepancies can be partially explained by interactions between alkali promoters and the iron species present in the catalyst, whose nature is not well known up to the moment. The increases in activity and selectivity are often explained in terms of the electropositivity, which would produce a charge transfer from alkali promoter to transition metal surface, inhibiting H_2 adsorption but enhancing CO adsorption and dissociation [8]. The role of potassium to increase the selectivity to heavy hydrocarbons was recently investigated by Pendyala [9] using TPR-EXAFS/XANES-TPR experiments. A possible electronic effect, reflected by a systematic increase in the carburization speed when the promoter basicity increases in precipitated (Fe: Si: alkali) catalysts, is showed. Accordingly, Li [10] concluded that potassium promotes new active sites production during carburization and reduction steps of precipitated iron oxides,

assisting a rapid nucleation to generate small iron carbides crystallites. In similar way, Ribeiro et al. [11] investigated the promoter effect of Li, Na, K, Rb, and Cs on the carburization rate in precipitated Fe-Si catalysts using X-ray absorption spectroscopy. They found that the carburization rate was increased in the following order: unpromoted < Li < Na < K = Rb = Cs. On the other hand, Xiong, et al. [12] studied the effect of group I alkali metals on Fe/carbon nanotubes catalysts in Fischer-Tropsch synthesis. They found that Li enhanced in a small extent the reducibility of the catalyst whereas Na and K slightly inhibited its reduction.

In summary, there is not a general agreement about the influence of alkali promoters on the performance of iron catalysts in FTS. An additional difficulty appears as consequence of the diverse structural properties of the different class of iron catalysts used: low specific surface in fused systems, presence of textural promoters in precipitated solids or system of nanoparticles on different types of supports.

Currently, there is a special attention on iron supported catalysts. They have greater resistance to attrition than bulk catalysts. This advantage allows their use in low cost reactors, such as slurry type. Therefore, is attractive to develop Fe supported catalysts with good activity and selectivity. However, this type of solids introduces new challenges in order to interpret the results because there is some earlier evidence that FTS is a "structure sensitive" reaction [13, 14]. That means that the activity and selectivity of the catalyst is a function of the crystal size of the active phase (generally in the range of 1- 10 nm). Recently, this property was confirmed for Co and Fe supported catalysts [15-18]. In this way, it would be possible to increase the selectivity of FTS by two effects: obtaining supported iron oxide nanoparticles with a determined average diameter and a narrow size distribution and using metal alkali as promoters. In order to "tailor" the size and the width of size distribution, an "inert" support with a narrow pore size distribution and thermal stability must be selected. In addition, the pore diameters must be large enough to locate the iron oxide crystals inside them, avoiding their migration to the external surface during the activation and the use steps. These conditions seem to be fulfilled by the mesoporous solid named SBA-15. It has a narrow pore-size distribution with a hexagonal arrangement, whose diameters can be varied between 5 and 30 nm, a wall thickness between 3 and 6 nm, and specific surface area between 700 and 1000 m^2/g [19, 20]. Several methods to incorporate Fe to SBA-15 have been studied [21] such as post-synthesis methods and co-condensation of Fe species with silica. These different methods lead to distinct kind of bonding and environments of Fe into the silica network. Wang [22] showed an increase in the hydrothermal stability of SBA-15 by incorporating Fe in the synthesis process. They claimed that Fe atoms are dispersed and anchored in the SBA-15 network producing a strengthening of their structure. The use of this type of support is not enough to obtain a narrow crystal-size distribution in the desired size range of the active Fe species. In order to reach this purpose, it is necessary to introduce the total iron loading inside the support channels avoiding its migration to the external surface when the catalyst is "working". Otherwise, the controlling effect on the sintering process would be lost. Achieving these objectives represents a real challenge.

Other support, with similar SBA-15 structural properties, that would fulfill with the previously mentioned requirements, would be the carbon ordered mesoporous named CMK-3. This solid is obtained by the nano-casting technique using SBA-15 as template. Thus, recently Cheng et al. [23] reported the use of Fe/CMK-3 system doped with sodium to be used as catalyst to produce olefins from FTS. Although, they found an increase in olefin selectivity and chain growth probability, the production of inactive sodium-iron mixed oxides or carbides decreased the reaction rate. Subsequently, the de Jong´s Group published two articles studying the Fe/SBA-15 and Fe/CMK-3 systems doped with sodium and sulfur. In the first one [24] they described a poor performance of the Fe/SBA-15, presumably by formation of iron silicate. These authors attributed this disadvantage to the iron salt used in the impregnation step: ammonium iron citrate. On the other hand, they found interesting results with Fe/CMK-3 doped with sodium and sulfur with high selectivity towards lower olefins and low methane production. In the second article [25], these researchers carried on studying the Fe/CMK-3 catalyst. A novelty result get by this group is the beneficial effect of the controlled poisoning with sulfur to increase the selectivity to C_2-C_4 olefins. From many years sulfur has been considered damaging for iron catalysts in the FTS.

Considering the previous discussion, the aim of the present work was go in depth in the study of doped Fe/SBA-15 system with alkali metals obtaining different supports doped with Li, K and Cs in order to generate surface basic sites. These modified solids were used as supports for iron nanoparticles to produce doped Fe/SBA-15 catalysts in order to increase their activity and selectivity towards hydrocarbons in gasoline range when they are used in the FTS. Bearing in mind the consequence of the active crystal size on the catalytic results of this process, efforts were performed to control the average size and width of Fe active phase distribution.

Results and Discussion

The preservation of the structural properties of the mesoporous SBA-15, after incorporation of alkali metals, was verified by XRD and textural measurements and these results were reported in a previous publication [26].

The Fe impregnation treatment and the subsequent calcination in NO (1% v/v)/He flow, carried out to obtain the precursors: Fe/SBA-15, Fe/Li-SBA-15, Fe/K-SBA-15 and Fe/Cs-SBA-15 did not modified the structural properties of the mesoporous supports, as it was verified by XRD (Figure 1). The NO/He flow was selected because it has been demonstrated that calcination in NO flow produces, in the Co/SiO_2 system, Co nanoparticles with sizes significantly smaller if cobalt nitrate salt is used in the impregnation step [27, 28]. Besides, these authors obtained an important narrowing in particle size distribution when this gas was used instead of air. These results could be explained since NO is one of the nitrogen oxides produced during metal nitrates decomposition; therefore, if it is fed during the calcination process, the salt decomposition would occur in a controlled way and the clustering and growth of the nanoparticles would be avoided.

In Figure 2 are reported TEM micrographs in order to show the iron species location. Figure 2a corresponds to Fe/SBA-15 in dark-field mode. This Figure shows the presence of iron oxide nano-cylinders along SBA-15 channels. It can be seen that bright areas, corresponding to iron species, are aligned following the channels path. This is an evidence of the position of this species inside the SBA-15 pores. The length of 73 nano-cylinders was measured and a distribution of this dimension was obtained. The histogram of these sizes was fitted assuming a log-normal distribution and the average value obtained was of 7.6 ± 0.3 nm (Figure 3). Figures 2b and 2c belong to Fe/K-SBA-15 and Fe/Cs-SBA-15, respectively. These pictures were

obtained parallels to the axis of the support channels. There it can be observed the mouths of empty pores of SBA-15 (lightest zones) with a hexagonal arrangement and some pores flled with iron oxide (darkness regions). It can be noticed that filled channels are surrounding by several vacant pores.

Table 1 displays BET results and the metal content (Fe and alkali metals) of each precursor determined by AE and AA spectroscopy. The decline of Sg values could be attributed to two effects in the doped catalysts. The modification of SBA-15 with alkali metals, without iron, produced a decreasing of specific surface areas between 30 and 60% with respect to pure SBA-15 [26]. When the doped supports were loaded with iron species, this fall was increased reaching values of about 70% with respect to pure SBA-15. That is, in doped precursors the Sg decreasing is produced by the simultaneous presence of iron species and alkali metals. On the other hand, as it was detected by TEM micrographs, only some channels of SBA-15 were filled with iron oxides nano-cylinders. Instead, a great number of them remain empty. Therefore, in the evaluation of D_p from N2 adsorption measurement, using the BJH model, only these empty pores are taken into account and the average pore diameter remains unaltered.

Table I– Textural properties, Iron and alkali metal loadings for the precursors.

Sample	S_g (m^2/g)	D_P (nm)	V_P (cm^3/g)	e (nm)	Fe content (% w/w)	Alkali content (% w/w)
SBA-15	*893*	*8.2*	*1.09*	*6.8*	—	—
Fe/SBA-15	519	7.0	0.6	6.2	15.6	—
Fe/Li-SBA-15	287	8.2	0.6	4.2	9.7	0.11
Fe/K-SBA-15	309	7.0	0.4	5.6	12.5	0.40
Fe/Cs-SBA-15	371	7.2	0.5	6.0	12.2	2.17

S_g: Specific surface area
D_p: average pore diameter
V_p: specific pore volume
e: wall thickness

Table II shows the CO_2 adsorption results for each precursor expressed in μmol CO_2/m^2 exposed of precursor. It should be noted that SBA-15 support did not present CO_2 desorption. This fact denotes the absence of basic Lewis sites in the undoped support, in concordance with previous results [29].

It is observed that all precursors have three CO_2 desorption maxima in well-differentiated temperature ranges (Figure 4). These maxima correspond to CO_2 adsorbed on basic sites with different adsorption strength: weak, intermediate and strong. Bearing in mind that SBA-15 without dopants did not adsorb CO_2, the existence of these peaks in non-doped Fe/SBA-15 must be associated to the presence of iron oxide nanoparticles produced during the preparation of the precursors. Xu et al. have found that iron catalysts supported on silicalite showed two peaks at similar temperatures to the two first ones present in our precursors [30]. Besides, our peak at the highest temperature could be attributed to a fraction of smaller iron oxides nanoparticles with surface $O^=$ more coordinatively unsaturated.

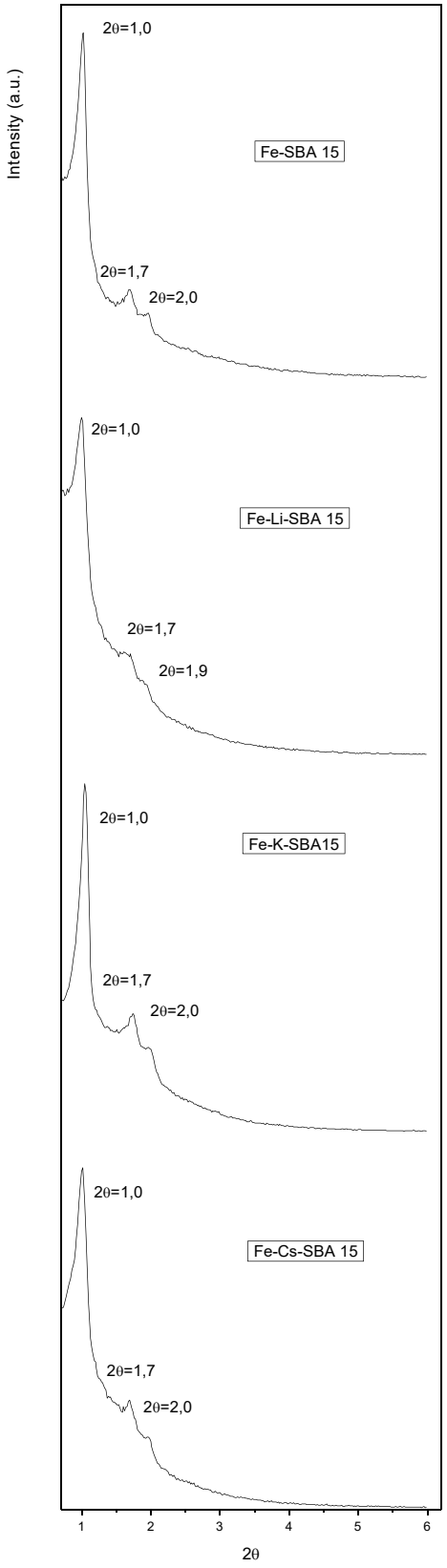

Figure 1: XRD patterns of precursors.

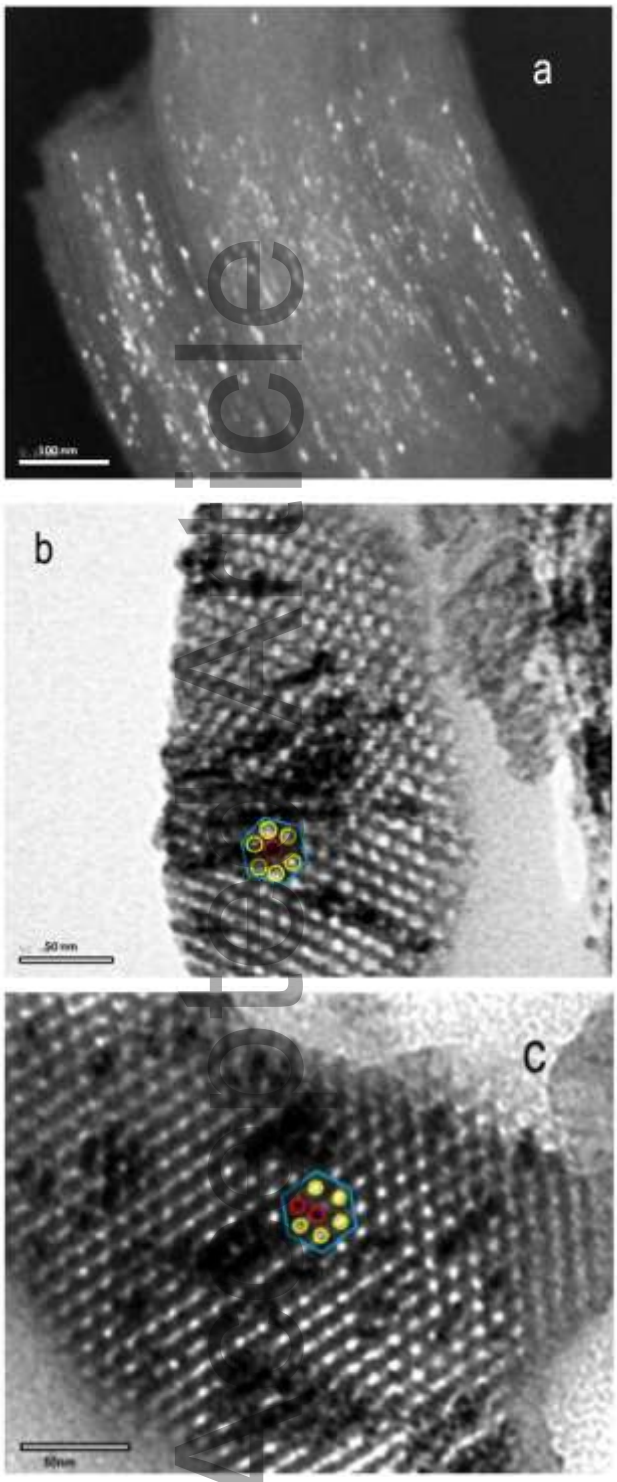

Figure 2: 2a: Dark-Field TEM of Fe/SBA-15 precursor. Light zones correspond to iron oxides nanoparticles inside the channels of SBA-15.**2b**: TEM of Fe/K-SBA-15 precursor. Light zones correspond to SBA-15 channels and dark zones to iron oxides. In a detail, inside light blue hexagon, red circle highlights a filled pore with iron species and yellow circles point empty channels.**2c**: TEM of Fe/Cs-SBA-15 precursor. Light zones correspond to SBA-15 channels and dark zones to iron oxides. In a detail, inside light blue hexagon, red circles highlight filled pores with iron species and yellow circles point empty channels.

Comparing with the CO_2-TPD results of SBA-15 without iron and doped with alkali metals (which only showed the two first peaks [26]), it can be concluded that the peak detected at higher temperature in doped precursors is produced exclusively by the presence of iron oxides nanoparticles.

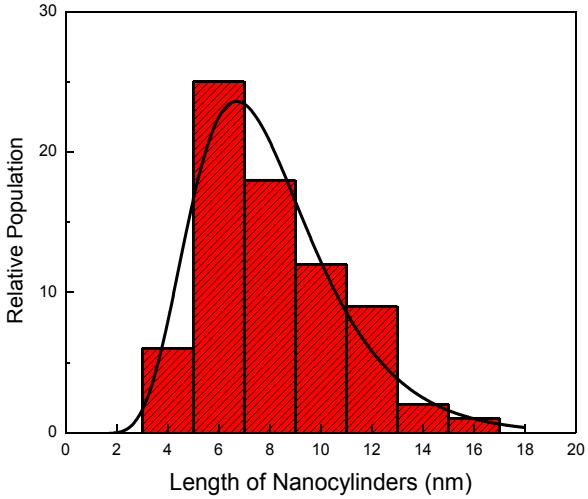

Figure 3: Iron nano-cylinders lengths distribution.

On the other hand, the peaks at low and medium temperatures detected on the doped precursors, can be attributed to the presence of alkali metals of group 1 located on the support surfaces [31]. Obviously, in these doped precursors the effect of the iron oxide microcrystals is also present but these adsorption quantities are negligible in comparison with that produced by the alkali doping agent. It must be remarked that all basic sites provided by the iron oxides will not have any influence during the catalytic reaction since the activation treatment with H_2 eliminates the isolated $O^=$ superficial, responsible for their presence. In this way only the weak and intermediate basic sites will be considered in the discussion.

Taking into account that the area obtained for each desorption peak is indicative of the amount of adsorbed CO_2 on the basic sites and normalizing by total surface area exposed (Table II) it can be concluded that the order by number of (weak + medium) basic sites obtained is: Fe/Li-SBA-15≅Fe/K-SBA-15>>Fe/Cs-SBA-15.

When CO_2 is adsorbed on alkali metals different species could be produced but the adsorption of one molecule of CO_2 always corresponds to one surface alkali metal atom [32-35]. If the amount of CO_2 molecules adsorbed per gram of solid is related to the total number of atoms of alkali metal per gram of solid, a rough estimation of the alkali metal dispersion could be obtained. These values would be independent of the amount of alkali metal added to each sample. When these calculations were performed it was found that K presents approximately twice times more dispersion than Li and eight times more than Cs (Table II). Two effects could be expected when the size of the alkali cations increases: a greater agglomeration degree of the species and/or a higher number of alkali ions located inside the walls of the SBA-15. These ions will be inaccessible to CO_2. The introduction of a fraction of the alkali cations into the walls of the SBA-15 is coherent with the lattice parameter change detected by XRD and with the densification of the SBA-15 network. However, the solid doped with K did not follow this tendency because it has the higher dispersion. In a previous work, performing XPS measurements, we found that Li, K and Cs are present as Li_2O, KOH and $CsNO_3$ respectively on the SBA-15 surface [26]. Taking into account that the melting points

of these compounds are: Li_2O: 1711 K, KOH: 633 K and $CsNO_3$: 687 K and that the precursors were calcinated at 723 K, could be speculated that KOH melted during this step of preparation producing a spreading on SBA-15, increasing its dispersion.

Table II. CO_2-TPD results of the precursors.

Precursor	1st Peak		2nd Peak		3rd Peak		CO_2 uptake of (1+2) peaks	Alkali metal dispersion (%)
	T (K)	Evolved CO_2 ($\mu mol/m^2 \times 10^4$)	T (K)	Evolved CO_2 ($\mu mol/m^2 \times 10^4$)	T (K)	Evolved CO_2 ($\mu mol/m^2 \times 10^4$)	($\mu mol/m^2 \times 10^4$)	
Fe/SBA-15	369	1.0	614	2.1	835	3.7	3.1	
Fe/Li-SBA-15	358	23.0	441	28.0	608	7.0	51.0	0.7
Fe/K-SBA-15	319	20.0	363	30.0	547	21.0	50.0	1.5
Fe/Cs-SBA-15	320	3.8	356	4.3	596	4.0	8.1	0.2

Using the maxima temperatures of CO_2 desorption peaks a qualitative order of the strength of the basic surface sites was estimated. If this value is high, the CO_2 desorption heat is greater and the basic strength of the site where the molecule was adsorbed is greater too [36]. According to the literature, an increase in the basic strength would be expected when the atomic weight of the alkali metal increases, but our results shows the following site strength order: Fe/Li-SBA-15>Fe/K-SBA-15 ≈ Fe/Cs-SBA-15. Comparing the three supports obtained in this work the Li-SBA-15 support is the one that exhibits the greatest basic strength for both weak and intermediate sites. In previous works, it has been reported that the Li generates more basic and stronger sites than expected [31,37].

To get more information about the structural properties of these precursors, the diffractograms of all of them at high angles (2θ = 5-90°) are reported in Supplementary Information. The poor quality of these patterns was determined by the characteristics of the samples. As it can be seen in Figure 1SI, a broad diffraction peak at about 2θ = 24°, typical for a highly disordered SiO_2 phase of SBA-15 [38], prevail in all solids. Besides, other two diffused peaks, in position compatibles with iron oxides can be detected ($2\theta \cong 33°$ and $2\theta \cong 62°$). The pronounced broadening and the scarce definition of these signals prevent to estimate crystallite size from the results of this technique. Notwithstanding, it can be concluded, at least in a qualitative way, that the iron species are present as very small nanoparticles. This conclusion is coherent with TEM results as it was previously explained.

Signals, attributable to Li_2O and KOH, were not detected and only one peak, that could belongs to $CsNO_3$, was visible at 2θ = 44.5°. It must be remember that, in order to maintain the Fe/M (M: alkali metal) atomic ratio constant, the weight percentage of cesium is about 20 times higher than that the lithium and 5 times than potassium. This fact would justify the detection of this peak.

Mössbauer spectroscopy of fresh catalysts

Figure 5 displays the Mössbauer spectra of the activated and fresh catalysts (at zero reaction time) at 298 and 30 K. All of them were registered in hydrogen atmosphere using the cell mentioned in Experimental Section with the aim to avoid the air contact and possible re-oxidations. The Mössbauer spectrum of activated Fe/SBA-15 at 298 K displays an asymmetric doublet with a shoulder at the positive velocities side, and broad lines that could be attributed to paramagnetic and/or superparamagnetic species (sp). In order to obtain a more precise species assignments the spectrum at 30 K was acquired.

It must be remarked that due to the high complexity of the spectrum at 30 K a conventional fitting process was not carried out. In a first step a set of hyperfine parameters, typical of the species that could be present, was fixed and the areas were fitted freely. Once these areas converge to a minimum, they were fixed and the isomer shift (δ) and quadrupole splitting (Δ) of the doublets and the hyperfine magnetic field (H) of the sextuplets were fitted freely. A decreasing in the hyperfine magnetic fields due to crystal size effects was considered. Instead, the isomer (δ) and quadrupole (2ϵ) shifts were fixed taking into account that they cannot be affected by the crystal size. Maybe the fittings obtained with this methodology lead to several minima, but they will have very small differences between them. In order to select the best set of values, the sample story and chemical and physical concepts were considered too.

Mössbauer parameters are displayed in Table A of supplementary information. In Table III are shown the percentages of each iron species present in the fresh activated catalysts. The spectrum at 30 K was fitted with six sextuplets and two doublets. Five of these sextuplets can be assigned to the five crystallographic Fe_3O_4 sites [39]. The additional sextuplet has hyperfine parameters characteristics of α-Fe [40]. Finally, the two doublets can be attributed to Fe^{+2} ions located in tetrahedral and octahedral sites inside SiO_2 walls of SBA-15 [40].

The same species are present as paramagnetic or in a superparamagnetic (sp) regime in the spectrum at 298 K. In this way, it can be detected two singlets corresponding to superparamagnetic α-Fe [40] and Fe_3O_4 [41] and two doublets assigned to paramagnetic Fe^{2+} ions diffused inside the silica walls and/or Fe_3O_4 (sp).

It can be concluded that only about 10% of the total iron loading could be reduced beyond Fe_3O_4 or Fe^{+2}. Besides, an important diffusion of iron ions inside SBA-15 walls occurs during the activation step. Bearing in mind that before activation only 4% of the total iron loading has diffused inside the walls [42] it could be inferred that two competitive routes would exist during sample reduction: one of them lead, as a final product, to α-Fe and the other produces Fe^{2+} ions, which diffuse very quickly inside the SBA-15 walls, and are stabilized there. Considering the final

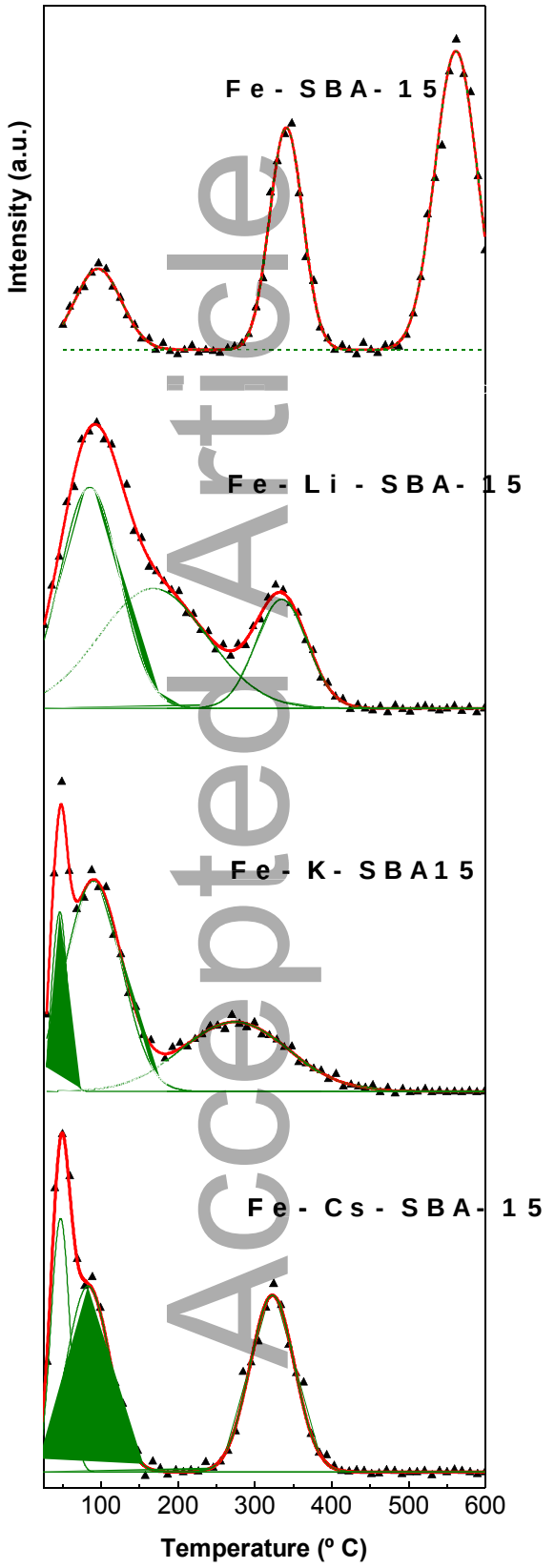

Figure 4: CO_2-TPD results of the precursors

species percentages, it can be concluded that the diffusion process is faster than the total reduction. Besides, as all species are superparamagnetic at 298 K, a migration of the nanoparticles outside the SBA-15 channels with sintering could be discarded.

Table III - Percentages of the species present in the activated catalysts at 30 K.

Species (%)	Fe/SBA-15	Fe/Li-SBA-15	Fe/K-SBA-15	Fe/Cs-SBA-15
α-Fe	11 ± 2	7 ± 1	8 ± 1	3 ± 1
Fe_3O_4	42 ± 13	65 ± 6	51 ± 2	74 ± 4
Fe^{+2}	47 ± 4	—	—	—
Fe_2SiO_4	—	22 ± 4	41 ± 4	23 ± 5

The spectra of the activated samples doped with alkali metals at 30 K are extremely complex due to the large number of peaks and to the presence of superparamagnetic relaxation as it can be inferred by the curved background even at this low temperature (Figure 5). Following the same methodology used for Fe/SBA-15 the spectra were fitted with five sextuplets of magnetically blocked Fe_3O_4 [39], one sextet of α-Fe and two doublets of Fe^{2+} ions located in tetrahedral and octahedral sites of the silica walls. However, this procedure did not produce a satisfactory fit. Therefore, it was considered that new species could be present in comparison with Fe/SBA-15 system. Taking into account the chemical elements present in the sample and the treatments carried out, it was proposed that this new species could be fayalite (Fe_2SiO_4). This compound crystalizes in an orthorhombic system with a distorted compact hexagonal packing of oxygen ions. Fe^{2+} ions occupy half of octahedral sites while Si^{4+} ions occupy 12.5% of the tetrahedral sites. Fe^{2+} ions are in two different crystallographic sites M_1 and M_2. At room temperature the Mössbauer spectrum shows an asymmetric doublet with different intensities and line widths indicating the presence of two doublets one per each site [43]. However, they are highly overlapped and cannot be distinguished during the spectrum analysis. When the temperature is lower than 65 K a magnetic ordering is produced, and a sextuplet and an octet appear. M_2 site produces eight lines because the electric quadrupole gradient is so intense (due to site distortion) that it cannot be considered as a hyperfine magnetic field perturbation. As consequence, magnetic quantum numbers are not "good numbers", the transition selection rules ($\Delta m = 0; \pm 1$) are not valid and forbidden transitions may occur ($\Delta m = \pm 2$). Bearing in mind these considerations, the fitting at 30 K was carried out with the same interactions than Fe/SBA-15 but a sextuplet and an octet were included instead of the two doublets of Fe^{2+} ions. To simulate the octet, eight Lorentzian lines were used which were combined in order to generate the corresponding hyperfine parameters using the methodology proposed by Kündig [44] who obtained graphics that allow evaluate H and 2ε for any combination of hyperfine magnetic fields and electric quadrupole gradients. There are a satisfactory agreement between the hyperfine parameters obtained from the fitting for both magnetic signals (sextuplet and octet) and that reported in bibliography for Fe_2SiO_4 [45]. From these results can be concluded that a superficial compound like fayalite has appeared in the SBA-15 pore walls due to an important Fe^{+2} diffusion inside them during the reduction step. Considering that in precursor the amount of

Fe^{3+} diffused inside silica walls is about 4 % [42] this migration is produced during the reduction step and competes with α-Fe formation.

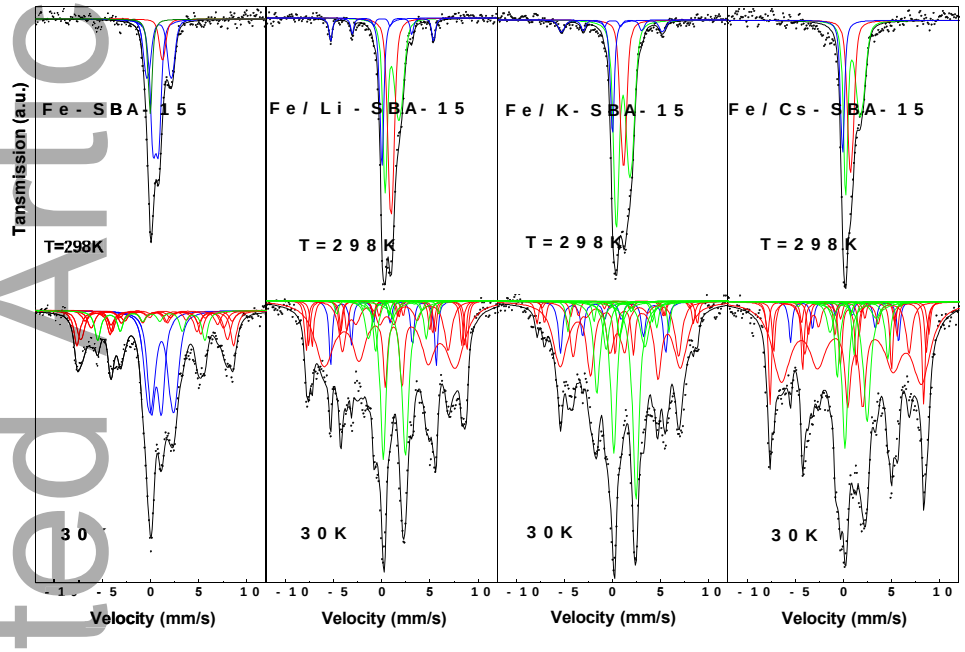

Figure 5: Mössbauer spectra of activated catalysts

It must be remarked that the total amount of Fe^{2+} diffused in the support walls in Fe/K-SAB-15 is similar to that detected in Fe-SBA-15 while in Fe/Li-SAB-15 and Fe/Cs-SAB-15 these quantities are lower than in non-doped catalyst. However, in absence of alkali metal, Fe^{2+} ions are not magnetically coupled at low temperature. This result would indicate that in Fe-SBA-15 the interatomic distance between iron ions is higher than in alkali metal promoted catalysts. It could be interpreted considering that Fe-SBA-15 has a homogeneous Fe^{2+} ions distribution inside SiO_2 walls. Instead, in promoted catalysts there would be regions where Fe^{2+} ions are more concentrated allowing the magnetically coupling at low temperature. It could be speculated that this Fe^{2+} heterogeneous distribution may be due to the presence of alkali metal ions inside the silica walls as it was demonstrated by XPS measurements [26], the dispersion values obtained from CO_2-TPD and by the methodology used in the doped support preparation. Therefore, inside the SBA-15 walls there would be regions where are located the alkali ions, leading to a strong electrostatic repulsion of Fe^{2+} ions. As consequence these ions would be concentrated in other zones favoring the magnetic coupling leading to fayalite formation.

The remaining signals were fitted in the same way that Fe-SBA-15: five sextuplets corresponding to magnetically blocked Fe_3O_4 and one sextet to α-Fe. Some differences with non-doped catalyst are an over-reduction of the Fe_3O_4 and a slight diminution of α-Fe production (this is more notorious in the catalyst doped with cesium).

The Mössbauer spectra at 298 K of doped catalysts indicate that all iron species present at 30K are detected at room temperature in a superparamagnetic regime. The three spectra were fitted with two singlets and one asymmetric doublet (Figure 5), Table A of supplementary information). The singlet with higher δ was assigned to superparamagnetic Fe_3O_4 [41] and the other one could be assigned to superparamagnetic α-Fe [40]. The asymmetric doublet is the convolution of the signals corresponding to Fe^{2+} ions in two different crystallographic sites, M_1 and M_2, of fayalite. They are highly overlapped and it is not possible to distinguish them from each other in the spectrum analysis.

Finally, in Fe/Li-SBA-15 and Fe/K-SBA-15 a small sextuplet with hyperfine parameters typical of α-Fe was detected. The presence of this signal would indicate certain sintering degree but their percentage is extremely small and this effect could be neglected.

It was concluded that in all fresh catalysts α-Fe, Fe_3O_4 and Fe^{2+} diffused inside the silica walls were detected. However, some differences must be remarked:

-the alkali metals presence hinder the iron reducibility, decreasing the α-Fe percentage and increasing the presence of over-reduced Fe_3O_4 one, which is an intermediate during reduction step. This result is more evident in Fe/Cs-SBA-15.

Other authors have found similar results [46]. This behavior allows us to infer that there is an interaction between Fe species and surface alkali metals;
-in presence of alkali metals, Fe^{2+} ions diffused inside SBA-15 walls are close enough to be magnetically coupled and produce a silicate (Fe_2SiO_4) instead of isolated paramagnetic Fe^{2+} ions as it was discussed above;
- at 298 K in Fe/SBA-15 and Fe/Cs-SBA-15 all iron species present have a superparamagnetic behavior while in Fe/Li-SBA-15 and Fe/K-SBA-15 a negligible fraction of α-Fe is magnetically blocked. Therefore, considering that the channel diameters of the supports have about 8nm it is possible to conclude that the active phase crystals have a controlled size below this value in all catalysts.

Mössbauer spectroscopy of used catalysts

In order to determine the iron species present in "working" catalysts, possible crystal size changes during reaction and the influence of the different alkali metals present in support, Mössbauer spectra of catalysts used in FTS during 24 h were collected at 298 and 30 K. Previously, it was verified that this time is enough to reach the pseudo-stationary state for all catalysts. All spectra were registered in the same atmosphere of the catalytic reaction using the cell described in Experimental Section with the aim to avoid the air contact and possible re-oxidations.
All spectra of the used catalysts, obtained at 298 K, looks similar to that of the fresh catalysts displaying an asymmetric doublet with broad lines and a shoulder on the positive velocities side, which could be attributed to paramagnetic and/or superparamagnetic species (sp). Only Fe/K-SBA-15 displays some different aspects as it will be described below.
However, the spectra at 30 K showed appreciable differences in comparison with that obtained for fresh catalysts at the same temperature (Figure 6). Table B of Supplementary Information displays hyperfine parameters obtained using the same fitting methodology that in fresh catalysts and Table IV shows the Fe species percentages of the catalysts at the pseudo-stationary state obtained from the Mössbauer spectra at 30K. In order to get a satisfactory fitting six sextuplets and two doublets were used. The two sextuplets with higher magnetic hyperfine fields can be assigned to Fe_3O_4 magnetically blocked. The percentage of this species decreased in all catalysts to a range of about 20 to 30 %. We considered inadvisable to use several interactions to distinguish the different crystallographic sites of Fe_3O_4 with these signals poor defined. Instead, only two sextuplets were used, each one represents the average "weighted" population of different sites of Fe^{3+} and Fe^{2+} respectively. It must be remarked that, in comparison with fresh catalysts, magnetite has been oxidized in all used catalysts increasing its Fe^{3+} percentages. The FTS atmosphere can be oxidant or reducing depending on CO, H_2, CO_2 and H_2O mole ratio. The amounts of these species are related to syngas conversion level and to the secondary reactions of "water-gas shift" and Boudouard. Our results indicate that with these catalysts and the operative conditions used the reaction atmosphere was oxidant.

Table IV - Fe species percentages of the catalysts at the pseudo-stationary state obtained from the Mössbauer spectra at 30K.

Species	Fe/SBA-15	Fe/Li-SBA-15	Fe/K-SBA-15	Fe/Cs-SBA-15
Fe^{+2}	34 ± 2	49 ± 2	47 ± 1	80 ± 3
Fe_3O_4	27 ± 2	24 ± 3	29 ± 1	16 ± 3
χFe_2C_5 + ε` $Fe_{2.2}C$	39 ± 5	27 ± 5	24 ± 1	4 ± 2

The remaining four sextuplets, with small hyperfine magnetic fields, can be assigned to three sites of χ-Fe_2C_5 carbide [47] and two sites of ε`-$Fe_{2.2}C$ carbide [48]. The signals corresponding to sites II of χ carbide and I of ε carbide are completely overlapped at low temperature. For this reason the carbide signals were fitted with four sextuplets instead of five. For Fe/Cs-SBA-15 very small amounts of carbide were detected, and the signals belonging to site III of χ carbide and site II of ε -$Fe_{2.2}C$ are below the error limits. Therefore these signals were not included in fitting.
Analyzing the results it can be observed that for Fe/Li-SBA-15 and Fe/K-SBA-15 the carbide total amount (27 ± 5 % and 24 ± 1 % respectively) exceeds the α-Fe percentages detected in fresh catalysts (7 ± 1 % for Li and 8 ± 1 % for K, respectively). In this way, it could be concluded that the carbide not only is produced from α-Fe but also from Fe_3O_4 whose percentage decreases. Similar result was obtained in Fe/SBA-15. However, as in Fe/Cs-SBA-15 the total carbide amount detected (4 ± 2 %) is equal to the α-Fe percentage obtained in the fresh solid it can be concluded that in this catalyst, the carbide is exclusively produced from α-Fe. Several authors have found that "working" catalysts have a mixture of iron carbides and oxides [49-54]
Finally, the two doublets can be assigned to Fe^{+2} ions in tetrahedral and octahedral sites inside SiO_2 walls [40] (Figure 6, Table IV). Is important to remark that in all doped fresh catalysts the Fe^{2+} ions had produced superficial fayalite. However, in the used catalysts they are present as isolated paramagnetic ions. This result would indicate that these ions have mobility and under the FTS a more homogeneous redistribution of them could occur. In this way, interatomic distances increased, and the magnetic coupling could not take place leading to isolated paramagnetic ions instead of fayalite.
Other interesting result is that, for Fe/K-SBA-15, the Fe^{+2} percentages is the same to that found in the fresh catalyst. However, for Li and Cs these values were considerably increased in the used catalysts, changing from 22 ± 4 % to 49 ± 2 % in Fe/Li-SBA-15 and from 23 ± 5 % to 80 ± 3 % Fe/Cs-SBA-15. These ions are inactives in the FTS, therefore this change produced by the presence of Li and Cs is undesirable.

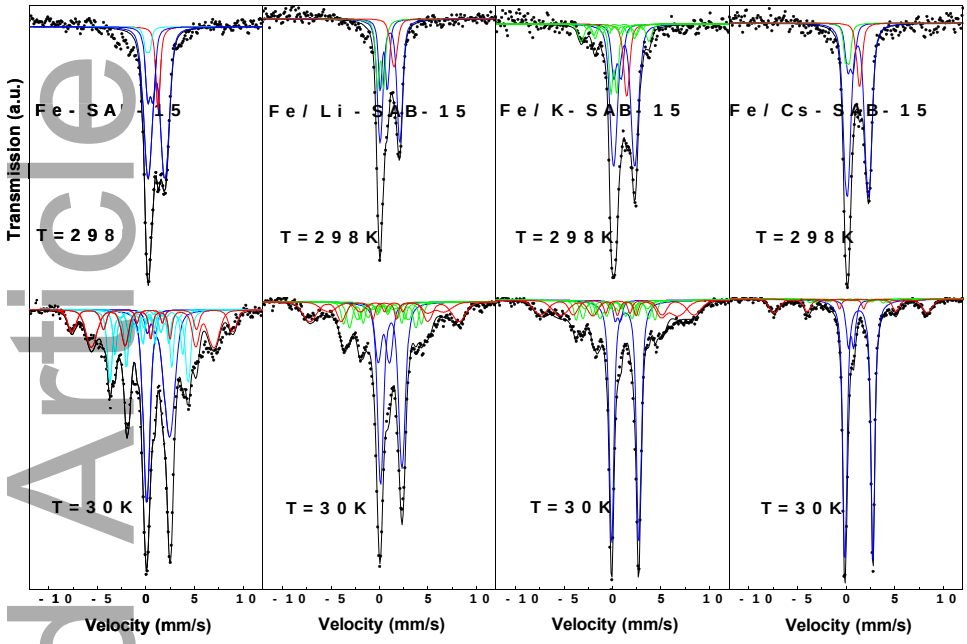

Figure 6: Mössbauer spectra of used catalysts.

On the other hand, the great increase in quadrupole splitting of Fe^{2+} located in octahedral sites for Fe/K-SBA-15 and Fe/Cs-SBA-15, compared with the value obtained in Fe/SBA-15, is indicative that these sites are highly distorted. Thus, the presence of alkali ions inside SiO_2 network would have affected its structure strongly, verifying the location of the alkali metal inside by SBA-15 wall. This was not observed in Fe/Li-SBA-15 indicating that a much smaller amount of lithium is in the support walls. These results are in the same direction to that obtained by CO_2-TPD and by XPS [26].

After the species assignment from the results at 30 K, the spectra at 298 K were fitted with three doublets and one singlet. Doublets with higher isomer shift were assigned to paramagnetic Fe^{2+} in tetrahedral and octahedral sites of the silica walls. The other doublet, with lower isomer shift, was assigned to superparamagnetic carbide and the additional singlet to superparamagnetic magnetite [41].

Fe/K-SBA-15 spectrum at 298 K displays small differences with the other catalysts. In this way, small and poor defined magnetic interactions can be seen at both sides of the central signals. Therefore, three additional sextuplets were added in fitting. They were assigned to I, II and III sites of χ-Fe_2C_5 carbide [47] and to site II of ε`-$Fe_{2.2}C$ which overlaps with site I of χ-Fe_2C_5 [48]. This fraction would be originated by carburization of the small percentage of α-Fe that would have migrated outside SBA-15 channels.

Therefore, all species detected at 30 K are present as paramagnetics or in a superparamagnetic regime in the spectra at 298 K. Besides, Fe-K-SBA-15 displays a small magnetically blocked fraction at room temperature.

Comparing the doped catalysts with Fe-SBA-15, after 24 hours of FTS, it can be concluded that in all cases the species detected were ε`-$Fe_{2.2}C$, χ-Fe_2C_5, Fe_3O_4 and Fe^{2+} ions diffused inside SBA-15 walls. However, it is interesting to remark the following differences:

-Cs presence has an important negative effect on the structural properties, since Fe mostly migrates inside the support walls being inactive to FTS;

-Fe^{2+} ions diffused into SBA-15 walls have mobility and were redistributed, and as consequence fayalite (Fe_2SiO_4) disappeared leading to isolated paramagnetic Fe^{2+} ions in the same way that in non-doped catalysts;

-in catalysts doped with K and Cs the SiO_2 octahedral site environments have a large distortion in comparison with Fe-SBA-15. This result is coherent with the presence of alkali ions inside the support walls. This effect was not detected in Fe/Li-SBA-15.

Is necessary emphasizing that superparamagnetic behavior of fresh and used catalysts in Mössbauer spectroscopy, at room temperature, was used to determine the existence or not of iron species sintering. This procedure is substantiate in the sensitivity of this technique to detect small changes of size when these iron species (α-Fe, Fe_3O_4 and iron carbides) are present. Thus, nanoparticles of α-Fe of 6 nm show a singlet at 298 K, but when their size enlarge to 10 nm a sextuplet is produced [40]. Something similar happens when Fe_3O_4 nanoparticles increase the diameter from 5 to 10 nm [55]. Finally, for χ-Fe_2C_5, when the size of the nanoparticles change from 5 to 8.5 nm, a predominantly relaxing spectrum is completely blocked at room temperature [47].

Catalytic tests

Catalytic tests were carried out at 1 and 20 atm. It must be remarked that to get acceptable conversion levels at 1 atm were assayed several reaction temperatures and 703 K was chosen. This is a severe requirement in comparison with the temperature used in industrial conditions. Notwithstanding, the tests were performed in order to study and characterize the behavior of the different catalytic solids. Alkanes and alkenes up to C_{22} were detected as products and oxygenated compounds were not found. Figure 7 shows the CO conversion values measured at different reaction times at 1 atm for the four catalysts.

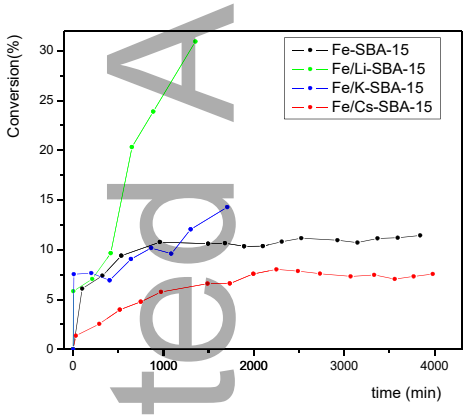

Figure 7: CO Conversion throughout the reaction time at 1atm.

Fe/SBA-15 and Fe/Cs-SBA-15 reach a pseudo-stationary state after approximately 24 h of reaction. In contrast, catalysts doped with Li and K shows a continuous conversion increase. Considering that pressure measurement instrument registered an increase of this variable, this result could be attributed to this effect. It is estimated that the presence of alkali metals on the catalyst surface favors the CO dissociation increasing its conversion (as it is explained below) but at the same time leads to an increase of secondary reactions such as the Boudouard reaction, which is also favored by the high reaction temperature. This reaction produces carbon, which obstructs the catalytic bed, increasing the system pressure. Confirming this reasoning, at the end of the tests a mass of compact coal was found in the catalytic bed when Fe/Li-SBA-15 and Fe/K-SBA-15 were used. In addition, during reaction the chromatographic analysis revealed the presence of a greater amount of CO_2 (the other product of the Boudouard reaction) when the catalysts used were those promoted with Li and K. For this reason, the comparisons between all the catalysts are accurate only at short reaction times (at about 8 h). Taking into account these considerations the following CO conversion order was found Fe/Li-SBA-15> Fe/K-SBA-15> Fe/SBA-15> Fe/Cs-SBA-15. Considering that the total number of basic surface sites created by doping with alkali metals follows the order: Li ≅ K >> Cs and that the strength order was: Li> K ≅ Cs, it is possible to infer that there would be a correlation between these results and the corresponding catalytic activities. Dissociation of CO, assisted by hydrogen or not, is generally seen as the first step in the reaction mechanism in the FTS [56]. Therefore, our catalytic results could be explained by electrostatic effects, of short- and long-range, generated by the alkali metals on Fe. These effects decrease the work function of iron and the bonding and antibonding molecular orbitals of CO fall below the Fermi level of the metal. As consequence, the antibonding level of CO becomes partially filled, and consequently the intramolecular bond is weakened, and its dissociation can be produced more easily [57, 58]. It important to remark that this model is based on experimental results and theoretical calculus for systems in which the alkali metals are deposited on the surface of the transition metals. However, in our case, basic sites were created on the surface of the SBA-15 support and then iron was deposited on this surface. Therefore, it could be deduced that the electrostatic effects have influence at a larger range than that "a priori" could be expected. As a general conclusion, higher quantity and strength of the basic sites make easier CO dissociation and the activity of the catalysts is increased. It also observed that Cs doped catalyst has activity even lower that Fe-SBA-15. In table III it can be seen that Fe/Cs-SBA-15 has the lowest α-Fe percentage of all fresh catalysts. In addition, this "working catalyst" has the greater fraction of Fe^{2+} ions diffused inside SBA-15 walls. Therefore, although Cs contributes with a promoter effect due to the presence of the alkali ions, the decrease of the reducibility degree and the increase of the percentage of species catalytically inactive predominate.

The selectivity results were expressed as Olefin/Paraffin ratio up to C_3 and up to C_{13}. Methane was not included for selectivity calculus. The comparison between all catalysts was carried out at iso-conversion values in order to discard effects of this variable on selectivity results (Table V).

Table V -Olefin / Paraffin ratio at isoconversion

Catalyst	CO conversion (%)	Olefin/Paraffin up to C_3 (without C_1)	Olefin/Paraffin up to C_{13} (without C_1)
Fe/SBA-15	9	1,6	1,6
Fe/Li-SBA-15	10	2,2	2,2
Fe/K-SBA-15	10	3,0	2,0
Fe/Cs-SBA-15	8	2,7	2,8

These results do not show a direct correlation with the number and strength of basic sites detected. Despite this complexity, it is possible to conclude that the presence of alkali dopants generates a beneficial effect on the olefins production in comparison with non-promoted catalyst. This result could be attributed to the negative charge densities generated on the basic sites (O^{2-}) produced by the presence of alkali dopants. In this way, olefins, which has high electron density in the double bonds, could be strongly repulse due to electrostatic effect and they would be quickly desorbed decreasing the hydrogenation probability to produce paraffins.

Selectivities for different hydrocarbon ranges at these iso-conversion values were also obtained (Figure 8). Light hydrocarbons in the range of C_2-C_4 were preferentially produced

by all catalyst. Fe/Li-SBA-15 shows the lower chain growth, and hydrocarbon production above C_{12} was not detected. On the opposite, Fe/Cs-SBA-15 showed the higher chain growth with an important selectivity in the range C_{13}-C_{18} (diesel) and even above C_{19}. However, an uncontrolled chain growth did not occur for any catalyst. The selectivity achieved on chain growth can be attributed to the control on the crystal size of the active species. The existence of shape selectivity due to support pores size cannot be completely discarded.

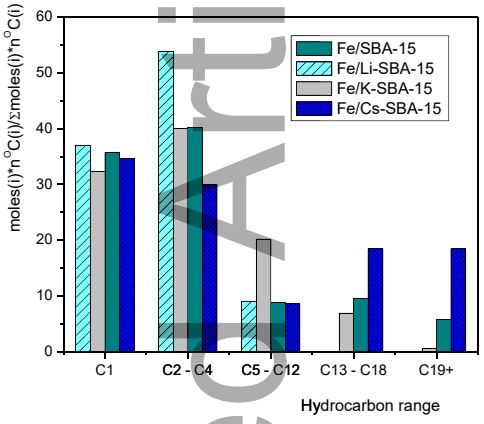

Figure 8: Selectivity to different hydrocarbons at iso-conversion.

The products obtained in catalytic tests at 20 atm and 543 K were alkenes and alkanes from methane up to C_{33}, oxygenated products were not found. The CO conversions, at different reaction time, are shown in Figure 9 for all catalysts. Bearing in mind the important diminution in the mole number, characteristic of the FTS, all of them showed a marked conversion increase with respect to the test at 1 atm. It must be highlight that at 1 atm a temperature of 703 K was necessary to get a CO conversion of about 10 %, instead at 20 atm, values in a range between 15 to 25% were obtained at only 543 K. In these conditions was no C formation or blockage of the catalytic bed in any case and an activity level approximately constant, during 48 h, was obtained. We consider that the pronounced difference between the necessary reaction temperatures at 1 and 20 atm is not only consequence of the change in the number moles during the FTS. Instead, we interpreted these results because of the presence of nanoparticles of the active species inside the channels of the SBA-15, which cause their occlusion. Considering that textural measurements indicate that only a fraction of the total channels are blocked, reactive and products could be going into and exit, respectively, thorough the micropores that connect empty mesopores with blocked mesopores. Considering the reduced diameter of the micropores this process could be controlled by diffusion and high temperatures are required at 1 atm. The increase of pressure allows to get a similar result but at a temperature considerably lower. A recent theoretical calculus indicates that, in a system of mesopores connected by micropores, effective diffusivities are increased 50 % when pressure is increased from 1 to 10 atm [59].

The activity order obtained was Fe/K-SBA-15> Fe/Li-SBA-15 ≅ Fe/SBA-15> Fe/Cs-SBA-15. This sequence is different to that obtained at 1 atm. Studies of infrared of CO adsorbed on transition metals promoted with alkali metals indicate that there is a remarkable weakening of C-O bond in the first layer of adsorbed molecules [58]. At higher coverages, other CO adsorption states are developed, and the softening of the C-O bond is considerably lower. We conclude that, at higher pressure, surface coverage is increased, and the promoter effect is attenuated.

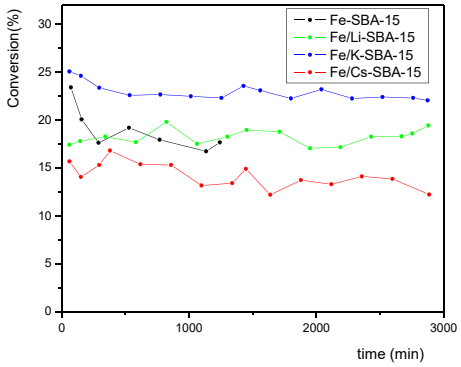

Figure 9: CO conversion at different reaction times in FTS at high pressure

At 20 atm was not possible to find iso-conversion values at any reaction time in order to carry out a reliable comparison of olefin selectivity. The most similar values found were 20% Fe/SBA-15, 19% Fe/Li-SBA-15, 22% Fe/K-SBA-15 and 15% Fe/Cs-SBA-15. Assuming that could be acceptable to make a comparison between the selectivity diagrams of the different catalysts at these conversion values, Figure 10 shows the percentage of the different hydrocarbon ranges, grouped in the same way as in tests at 1 atm. All catalysts show a low methane production compared with its behavior at atmospheric pressure. Besides, they principally produced light hydrocarbons (C_2-C_4) and, in comparison with test at 1 atm, an important increase is observed in gasoline range (C_5-C_{12}). The diesel (C_{13}-C_{18}) range fraction amount is very low. It is a very promising result that all catalysts show high selectivity towards gasoline range with values between 30 and 40%. This selectivity achieved on chain growth can be attributed to the crystal size control of the active species although the existence of shape selectivity due to the support pores sizes cannot be completely discarded. There is no noticeable effect in selectivity due to the presence of alkali promoters.

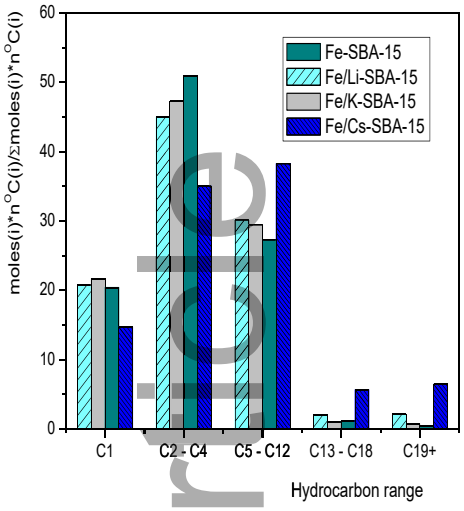

Figure 10: Selectivity to different hydrocarbons ranges.

Conclusions

A mesoporous solid SBA-15 was promoted with Li, K or Cs and then it was used as a support of iron. These composites were utilized as catalysts in the Fischer-Tropsch synthesis. We have proofed the creation of basic surface sites, with different quantities and strengths depending on the alkali metal, by CO_2-TPD. The dopant that has produced more sites and with greater strength was Li.

A detailed study of the catalysts after the activation step, in controlled atmosphere of H_2, indicates that α-Fe, Fe_3O_4 and Fe^{+2} diffused inside the SBA-15 walls are present in all them. However, the alkali metals produce some distinctive features. In this way, iron reducibility is hindered, decreasing α-Fe percentage and increasing that of Fe_3O_4, which is an intermediate in the reduction step.

On the other hand, in all "working" catalysts a mixture of carbides ε`-$Fe_{2.2}C$ and χ-Fe_2C_5, Fe_3O_4 and ions Fe^{+2} inside the SBA-15 walls were found. In comparison with fresh catalysts a re-distribution of Fe^{2+} ions and an oxidation of the Fe_3O_4 were detected. Both findings show that iron species are changing during the FTS. Besides, the increase of Fe^{3+} percentage in Fe_3O_4 indicates that the reaction atmosphere is oxidant.

The existence of all iron species, in fresh and in "working" catalysts, in a superparamagnetic regime at room temperature is indicative that activation step and the synthesis conditions did not produce sintering of them. Only Fe/K-SBA-15 showed a negligible fraction of iron carbides with magnetic blocking. Therefore, we can conclude that particle size effects are not present and the differences between catalysts could be attributed, exclusively, at the different alkali ions.

In the FTS at 1 atm the activity order obtained was: Fe/Li-SBA-15> Fe/K-SBA-15> Fe/SBA-15 > Fe/Cs-SBA-15. These results can be explained by an electrostatic effect generated by the alkali metals which decrease the work function of iron. We consider important to remark that the preparation sequences of doped catalysts should not lead to deposit the alkali metals on the surface of iron species. Notwithstanding, the electrostatic effects are reflected in the catalytic results. Therefore, it could be deduced that would not be necessary a physical contact between alkali metals and iron species to get promoter effects. Besides, it is possible to conclude that alkali dopants of Group 1 favored the olefins production.

An important conversion increase was observed when the catalytic tests were carried out at 20 atm. This is an expected result taking into account the considerable diminution in the mole number when the FTS occurs. However, we consider that other effect must be present because at 1 atm was necessary to use a temperature as high as 703 K to get an acceptable CO conversion. Instead, at 20 atm, a temperature of 543 K is enough to reach higher activity. We attributed this result to the fact that the iron nanoparticles located inside the SBA-15 channels would block the free movement of reactive and products. Considering that the mesopores of SBA-15 are connected between them by micropores and that only a portion of the mesopores are blocked, reactive could reach the active site across the empty mesopores and the micropores of the walls. At 1 atm this sequence would be slow and high temperatures would be necessaries to speed up the process. Instead, at 20 atm, effective diffusivities can be significantly increased, and the reaction would proceed satisfactory at low temperature. Other interesting aspect is that the difference between distinct dopants and the catalyst without promoter have decreased. Besides, all catalysts show low methane production, high selectivity towards light gases and an interesting production in the gasoline range between 30 and 40%. It should keep in mind that pressure and temperature used in these tests are like that used in industrial conditions. Therefore, these solids, especially Fe/K-SBA-15, would be promising to produce, with an acceptable level, hydrocarbons in the gasoline range. This selectivity, achieved on chain growth, can be attributed to the crystal size control of the active species although the existence of shape selectivity, due to the support pores sizes, cannot be completely discarded.

Experimental Section

Catalyst preparation

The SBA-15 support was synthesized according to the methodology proposed by Zhao et al. [19, 20] using Pluronic triblock copolymer P123 (EO_{20}-PO_{70}-EO_{20}) as organic structure-directing agent and tetraethyl orthosilicate (TEOS) as silica source. Thus, 12 g of Pluronic P123 were dissolved in a solution consisting on 60 ml of HCl solution (37% w/w) in 360 ml of water under stirring at 313 K during 3 h. Then, 27 ml of TEOS were added, and the resulting solution was kept under stirring at 313 K for 24 h. The mixture was statically aged at 363 K during overnight. The solid was recovered by filtration, washed, and dried in air at room temperature (RT). The sample was calcined in air flow (150 cm^3/min) heating from RT to 773 K at 1 K/min and kept at 773 K for 6 h. To obtain the promoted supports, Li-SBA-15, K-SBA-15 and Cs-SBA-15, this synthesis was slightly modified following a methodology developed in our laboratory. Together with P123, the corresponding alkali metal nitrate was added. Once the solid was obtained, the remaining water in the synthesis gel, was slowly evaporated in vacuum at 333 K in a rotary evaporator avoiding the filtration step. The alkali metal loadings on SBA-15 were established maintaining the Fe/M (M: alkali metal) atomic ratio constant and equal to that of the commercial catalysts in all samples [60]. All supports were impregnated by the incipient wetness impregnation method with $Fe(NO_3)_3 \cdot 9H_2O$ ethanolic solution to produce a nominal Fe loading of 15% w/w in a single step. The solids were dried using a rotary evaporator at 313 K for 24 h and finally calcined in NO/He (1% v/v) flow

(100 cm^3/min) from RT to 723 K at a heating rate of 1 K/min and kept at this temperature for 4 h. The samples thus obtained were called Fe-SBA-15, Fe/Li-SBA-15, Fe/K-SBA-15 and Fe/Cs-SBA-15.

Catalyst characterization

The samples were characterized by atomic absorption-emission spectroscopy (AA/AE), UV-Vis spectroscopy (UV-Vis), X-ray diffraction at low angles (XRD), transmission electron microscopy (TEM), N_2 adsorption (BET), Mössbauer spectroscopy (MS) and CO_2 desorption at programmed temperature (CO_2-TPD).

The alkali metal content of the solids was determined in a AA/AE Atomic Absorption Instrument Spectrophotometer 457 of Instrumentation Laboratory Inc., while the Fe content was determined in a UV-Vis spectrophotometer Perkim Elmer Lambda 35. The X-ray diffraction patterns at low angles were recorded in Shimadzu equipment, XD3A model, using Cu K_α radiation generated at 40 kV and 40 mA in the range 2θ = 0.5–6° with steps of 0.02° and counting time of 2 s/step.

For TEM measurements a JEOL model JEM-1200 EX II microscope was used. Samples for analysis were prepared by drying a dispersion of the solids on amorphous carbon coated copper grids

N_2 adsorption-desorption isotherms at 77 K were measured in a Micromeritics ASAP 2020 V1.02 equipment. The samples were previously outgassed at 523 K for 12 h. Textural properties, such as specific surface area (S_g), specific pore volume (V_p), and average pore diameter (D_p) were calculated from the experimental data. Combining XRD and BET techniques, the wall thickness (e) was obtained.

The Mössbauer spectra were acquired in transmission geometry with a 512 channels constant acceleration spectrometer. A ^{57}Co source in Rh matrix of nominally 50 mCi was used. Velocity calibration was performed using a 12 μm thick α-Fe foil. All isomer shifts (δ) mentioned in this work were referred to this standard. A closed cycle cryogenic system (DISPLEX DE-202) was used to modify the temperature between 30 and 298 K. The Mössbauer spectra were evaluated with a commercial fitting program named Recoil [61], using Lorentzian lines and all spectra were folded to minimize geometric effects. The spectra of fresh and used catalysts, in a controlled atmosphere of H_2 or in the reaction gases, respectively, were obtained using a special cell designed and built in our laboratory [62]. In this way the contact of the solids with air was avoided and possible re-oxidations, during the sample handling and the spectra measurement, can be discarded.

For the CO_2-TPD analysis the samples were activated “in situ” in Ar flow (20 cm^3/min) at 973K for 2 h, cooled to RT and then exposed to a stream of CO_2/Ar (8:100) to adsorb CO_2 until surface saturation. After that the sample was treated in pure Ar flow (90 cm^3/min) to remove the physisorbed CO_2. Then, it was heated in Ar flow (20 cm^3/min) at 10K/min up to 973K. The desorbed CO_2 was converted in CH_4 using H_2 flow (20 cm^3/min) and a Ni/SiO_2 catalyst at 673 K, then the CH_4 was quantified in a FID detector.

Activity and selectivity measurements

Activity and selectivity measurements at atmospheric pressure and 703 K were carried out in a stainless steel fixed-bed reactor, using H_2:CO flow with 2:1 molar ratio and a space velocity of 1176 h^{-1} (≈450 mg of catalyst and a total flow rate of 20 cm^3/min) . The catalysts were reduced “in situ” before reaction using hydrogen flow (99.999% purity), at atmospheric pressure and 703 K for 6 h. After the reduction treatment, H_2 flow was replaced by H_2:CO mixture and the catalytic test started. The products were analyzed "online" by gas chromatography using FID and TCD as detectors and two columns: capillary GS-Gas Pro and filled HAYESEP DB 100/120, respectively.

The FTS at high pressure was carried out in a unit of Iconel (Ni-Cr-Fe based alloy mainly) on a small scale. The gases used were: H_2 for sample reduction, N_2 for reactor purge and a mixture of 31.7% CO/ 64.3% H_2/ 4% He for the reaction. He was used as an internal standard to calculate the total CO conversion. The reactor was operated at a total pressure of 20 atm, a space velocity of 1176 h^{-1} (≈ 450 mg of catalyst and a total flow rate of 20 cm^3/min) and a reaction temperature of 543 K. The products were analyzed "online" by gas chromatography using FID and TCD as detectors and columns megabore CP-Sil 5 CB and filled CP-PoraBONDQ, respectively.

The different reaction temperatures used at high and low pressure are because at atmospheric pressure, catalysts need a high temperature to reach good conversion levels [16]. Instead, at 20 atm good activity levels are achieved at low temperatures.

Acknowledgements

The authors acknowledge the financial support of FONCyT-ANPCyT (PICT 2017-2808), CONICET and National University of La Plata which allowed the development of this work.

Keywords: Fischer Tropsch Synthesis • Mesoporous materials • Alkali cations • Basicity • Mössbauer spectroscopy

[1] Snehesh Shivananda Ail, S. Dasappa, Renewable and Sustainable Energy Reviews, 2016, 58 C, 267-286.
[2] J. Yang, W. Ma, D. Chen, A. Holmen, B.H. Davis, Appl. Catal. A: Gen., 2014, 470, 250-260.
[3] A.Y. Khodakov, W. Chu, P. Fongarland, Chem. Rev., 2007, 107, 1692–1744.
[4] W. Chen, T. Lin, Y. Dai, Y. An, F. Yu, L. Zhong, S. Li, Y. Sun, Catal. Today, 2018, 311, 8–22.
[5] J. Li, X. Cheng, C. Zhang, Q. Chang, J. Wang, X. Wang, Z. Lv, W. Dong, Y. Yang, Y. Li, Appl. Catal. A: Gen., 2016, 528, 131–141.
[6] Y. Yang, H.W. Xiang, Y.Y. Xu, L. Bai, Y.W. Li, Appl. Catal. A: Gen., 2004, 266,181–194.
[7] W. Ngantsoue-Hoc, Y.Q. Zhang, R.J. O’Brien, M.S. Luo, B.H. Davis, Appl. Catal.A: Gen., 2002, 236, 77–89.
[8] G. Zhao, C. Zhang, S. Qin, H. Xiang, Y. Li, J. Mol. Catal. A: Chem., 2008, 286,137–142.
[9] V.R.R. Pendyala, G. Jacobs, J.C. Mohandas, M. Luo, H.H. Hamdeh, Y. Ji, M.C.Ribeiro, B.H. Davis, Catal. Lett., 2010, 140, 98–105.
[10] S. Li, W. Ding, G.D. Meitzner, E. Iglesia, J. Phys. Chem. B, 2002, 106, 85–91.
[11] M.C. Ribeiro, G. Jacobs, B.H. Davis, D.C. Cronauer, A.J. Kropf, C.L. Marshall, J.Phys. Chem. C, 2010, 114, 7895–7903.
[12] H. Xiong, M.A. Motchelaho, M. Moyo, L.L. Jewell, N.J. Coville, Fuel, 2015, 150, 687–696.
[13] M. Boudart, A. Delbouille, J.A. Dumesic, S. Khammouma, H. Topsøe, J. Catal., 1975, 37, 486–502.
[14] M.A. McDonald, D.A. Storm, M. Boudart, J. Catal., 1986, 102, 386–400.
[15] E.I. Mabaso, E. van Steen, M. Claeys, DGMK Tagungsbericht, 2006, 4, 93–100.
[16] L.A. Cano, M.V. Cagnoli, N.A. Fellenz, J.F. Bengoa, N.G. Gallegos, A.M. Alvarez,S.G. Marchetti, Appl. Catal. A: Gen., 2010, 379, 105–110.
[17] P.B. Radstake, J.P. den Breejen, G.L. Bezemer, J.H. Bitter, K.P. de Jong, V.Frøseth, A. Holmen, Stud. Surf. Sci. Catal., 2007, 167, 85–90.
[18] G.L. Bezemer, J.H. Bitter, H.P.C.E. Kuipers, H. Oosterbeek, J.E. Holewijn, X. Xu, F.Kapteijn, A.J. van Dillen, K.P. de Jong, J. Am. Chem. Soc., 2006, 128, 3956–3964.
[19] D. Zhao, J. Feng, Q. Huo, N. Melosh, G.H. Fredrickson, B.F. Chmelka, G.D.Stucky, Science, 1998, 279, 548–552.
[20] D. Zhao, Q. Huo, J. Feng, B.F. Chmelka, G.D. Stucky, J. Am. Chem. Soc., 1998, 120, 24 6024-6036.
[21] F. Martinez, Y.J. Han, G. Stucky, J.L. Sotelo, G. Ovejero, J.A. Melero, Stud. Surf. Sci. Catal., 2002, 142, 1109-1116.

[22] X.Q. Wang, H.L. Ge, H.X. Jin, Y.J. Cui, Micropor. Mesopor. Mat., 2005, 86, 335-340.
[23] K. Cheng, V.V. Ordomsky, B. Legras, M. Virginie. S. Paul, Y. Wang, A.Y. Khodakov, Appl. Catal. A: Gen.2015, 502, 204–214.
[24] M. Oschatz, W.S. Lamme, J. Xie, A. I. Dugulan, K.P. de Jong, ChemCatChem, 2016, 8, 1–8.
[25] M. Oschatz, J.P. Hofmann, T.W. van Deelen, W.S. Lamme, N.A. Krans, E.J.M. Jensen, K.P. de Jong, ChemCatChem, 2017, 9, 620 –628.
[26] L. A. Cano, M. V. Cagnoli, J. F. Bengoa, J. L. Garcia-Fierro,S. G. Marchetti, J. Porous Mater., 2017, 24, 631–638.
[27] J.R.A. Sietsma, J.P. den Breejen, P.E. de Jongh, A.J. van Dillen, J.H. Bitter, K.P. deJong, Stud. Surf. Sci. Catal., 2007, 167, 55–60.
[28] J.P. den Breejen, J.R.A. Sietsma, H. Friedrich, J.H. Bitter, K.P. de Jong, J. Catal., 2010, 270, 146–152.
[29] S. Yang, W. Zhu, Q. Zhang, Y. Wang, J. Catal., 2008, 254, 251-262.
[30] L. Xu, Q. Wang, D. Liang, X. Wang, L. Lin, W. Cui, Y. Xu, Appl. Catal. A: Gen., 1998, 173, 19-25.
[31] V.K. Díez, C.R. Apesteguía, J.I. Di Cosimo, Catal. Today, 2000, 63, 53–62.
[32] R. Philipp, K. Fujimoto, J. Phys. Chem., 1992, 96, 9035-9038.
[33] J.I. Di Cosimo, V.K. Díez, M. Xu, E. Iglesia, C.R. Apesteguía, J. Catal., 1998, 178, 499-510.
[34] C. Morterra, G. Ghiotti, F. Boccuzzi, S. Coluccia, J. Catal., 1978, 51, 299-313.
[35] J.V. Evans, T.L. Whateley, Trans. Faraday Soc., 1967, 63 2769-2777.
[36] A.C.C. Chang, S.S.C. Chuang, M. Gray, Y. Soong, Energy Fuels, 2003, 17, 2, 468-473.
[37] T. Kanno, M. Kobayashi in Acid–Base Catalysts II, (Eds.: M. Misono, Y. Ono), Kodansha/Elsevier, Tokyo/Amsterdam, 1994, 207–211.
[38] S. Ganji, P. Bukya, V. Vakati, K. S. R. Rao, D. R. Burri, Catal. Sci. Technol., 2013, 3, 409-414.
[39] F.J. Berry, S. Skinner, M.F. Thomas, J. Phys.:Condens. Matter., 1998, 10, 215-220
[40] B.J. Clausen, H. Topsøe, Appl. Catal., 1989, 48, 327-339.
[41] S. Mørup, H. Topsøe, J. Lipka, J. Phys. Colloq., 1976, 37, C6-287-290
[42] L. A. Cano, M. V. Cagnoli, J. F. Bengoa, A. M. Alvarez, S. G. Marchetti, J. Catal., 2011, 278 310–320
[43] Vandenberghe, R.E.; "Mössbauer Spectroscopy and Applications in Geology". International Training Centre for Post-Graduate Soil Scientist, Belgium (1991).
[44] W. Kündig, Nuclear Instruments and Methods, 1967, 48, 219-228.
[45] G. Amthauer, W. Lottermoser, G. Redhammer, G. Tippelt, Hyperfine Interact., 1998, 113, 219-248.
[46] J. Li, X. Cheng, Ch. Zhang, Q. Chang, J. Wang, X. Wang, Z. Lv, W. Dong, Y. Yang, Y. Li, Applied Catalysis A: General 528 (2016) 131–141.
[47] S.Ch. Lin, J. Phillips, J. Appl. Phys., 1985, 58 (5) 1943-1949.
[48] M. Pijolat, V. Perrichon, P. Bussiére, J. Catal., 1987, 107, 82-91.
[49] R.B. Anderson in The Fischer-Tropsch Synthesis, Academic Press, New York (1984).
[50] J.A. Amelse, J.B. Butt, L.H. Schwartz, J. Phys. Chem., 1978, 82, 558-563.
[51] G.B. Raupp, W.N. Delgass, J. Catal., 1979, 58, 361-369.
[52] Dry, M. E. In: Catalysis, Science and Technology, (Eds.: J.R. Anderson, M. Boudart), Springer, Berlin Heidelberg New York 1981, VoL I, page 159.
[53] R.B. Anderson, in: Catalysis, 4th ed.(Ed.: P.H. Emmett), Van Nostrand-Reinhold, New York (1956) 29
[54] C.N. Satterfield, R.T. Hanlon, S.E. Tung, Z. Zou, G.C. Papaefthymiou, Ind. Eng. Chem. Prod. Dev., 1986, 25, 407-414.
[55] G. F. Goya, T. S. Berquó, F. C. Fonseca, M. P. Morales, J. Appl. Phys., 2003, 94, 5, 3520-2528.
[56] J. M. Gracia, F. F. Prinsloo, J. W. Niemantsverdriet, Catal. Lett., 2009, 133, 257–261.
[57] V. Bonacic-Koutecky, J. Koutecky, P. Fantucci, V. Ponec, J. Catal., 1988, 111, 409-417.
[58] J.W. Niemantsverdriet in Spectroscopy in Catalysis: An Introduction. Third edition, Wiley-VCH Verlag GmbH & Co. KGaA: Weinheim. 2007.
[59] P. Zeigermann, J. Kärger, R. Valiullin, Micropor. Mesopor. Mat., 2013, 178, 84–89
[60] M.E. Dry, Stud. Surf. Sci. Catal., 2004, 152, 533-600.
[61] K. Lagarec and D.G. Rancourt, "Mossbauer spectral analysissoftware". Dep. of Phys. University of Otawa , 1998, Version 1.0.
[62] I. Pérez De Berti, J. Bengoa, N. Fellenz, R. Mercader, S. Marchetti, Rev. Sci. Instrum., 2015, 86, 023903

Table of contents

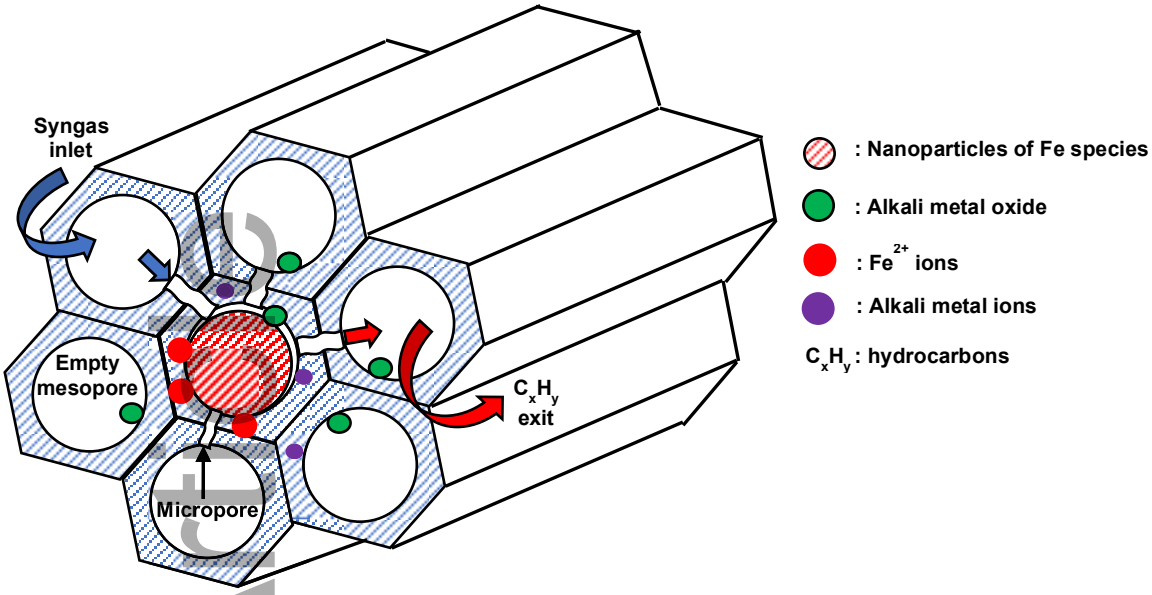

SBA-15 can be doped with alkali metals and used as support of iron species to obtain promising catalysts for Fischer-Tropsch synthesis. Consequences of promotion can be explained by the presence of surface basic sites and long-range electrostatic effects. Mesoporous channels are partially blocked by nanoparticles of iron species but reactive can achieve the active sites and products can be exit through micropores of SBA-15 walls.